Journal of Power Sources 451 (2020) 227765

Contents lists available at ScienceDirect

Journal of Power Sources

journal homepage: www.elsevier.com/locate/jpowsour

Bipolar electrochemical capacitors using double-sided carbon nanotubes on graphite electrodes

Josef Hansson [a,1], Qi Li [a,1,*], Anderson Smith [a], Isaac Zakaria [b], Torbjörn Nilsson [a], Andreas Nylander [a], Lilei Ye [c], Per Lundgren [a], Johan Liu [a,*], Peter Enoksson [a,*]

[a] Electronics Materials and Systems Laboratory, Department of Microtechnology and Nanoscience (MC2), Chalmers University of Technology, 412 58, Göteborg, Sweden
[b] Department of Chemical Engineering, University of California, Santa Barbara, 93106-5080, California, USA
[c] SHT Smart High Tech AB, Kemivägen 6, 412 58, Göteborg, Sweden

HIGHLIGHTS

- VACNTs are grown on both sides of graphite substrate in one-step CVD.
- Bipolar supercapacitor is fabricated with double sided graphite/VACNTs.
- State-of-art volumetric energy and power among CNTs based supercapacitors.
- Compact and low loss bipolar device is obtained without sacrificing stability.

GRAPHICAL ABSTRACT

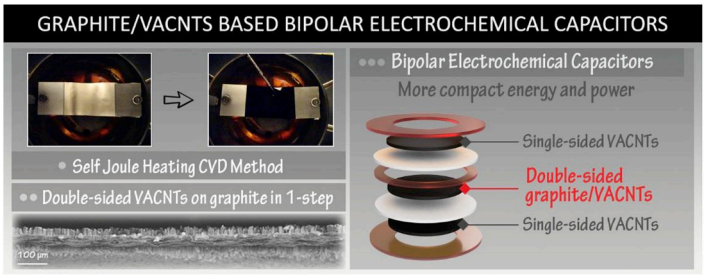

ARTICLE INFO

Keywords:
Self-joule heating
CVD
Supercapacitor
Bipolar
Series connection
Volumetric
Self-discharge
Miniaturized self-powered systems

ABSTRACT

The electrochemical capacitor (EC) is a key enabler for the miniaturized self-powered systems expected to become ubiquitous with the advent of the internet-of-things (IoT). Vertically aligned carbon nanotubes (VACNTs) on graphite holds promise as electrodes for compact and low-loss ECs. However, as with all ECs, the operating voltage is low, and miniaturization of higher voltage devices necessitates a bipolar design. In this paper, we demonstrate a bipolar EC using graphite/VACNTs electrodes fabricated using a joule heating chemical vapor deposition (CVD) setup. The constructed EC contains one layer of double-sided VACNTs on graphite as bipolar electrode. Compared to a series connection of two individual devices, the bipolar EC has 22% boost in volumetric energy density. More significant boost is envisaged for stacking more bipolar electrode layers. The energy enhancement is achieved without aggravating self-discharge (71.2% retention after 1 h), and at no sacrifice of cycling stability (96.7% over 50000 cycles) owing to uniform growth of VACNTs and thus eliminating cell imbalance problems.

1. Introduction

Miniaturized self-powered systems with harvest-store-use architectures have been recognized as a key enabler to the internet-of-things (IoT) [1,2]. Electrochemical capacitors (ECs), also known as supercapacitors, are characterized by an extremely long cycle life, high

* Corresponding authors.
E-mail addresses: qili@chalmers.se (Q. Li), johan.liu@chalmers.se (J. Liu), peter.enoksson@chalmers.se (P. Enoksson).
[1] These authors contributed equally to this work.

https://doi.org/10.1016/j.jpowsour.2020.227765
Received 16 October 2019; Received in revised form 21 December 2019; Accepted 16 January 2020
Available online 27 January 2020

power density and high coulombic/energy efficiency [3]. When utilized as energy storage units in miniaturized self-powered systems, these characteristics of ECs promise "fit and forget" maintenance-free networks with rapid energy storage/delivery at high efficiency.

Considering the need for integrating multiple electronics in a limited footprint and space to construct compact miniature smart systems, the form factor of the storage ECs is an important aspect to take into account. In this regard, micro-supercapacitors (MSCs), i.e. electrochemical micro-capacitors, with merits of miniaturization, flexible designs, and excellent integration compatibility are promising candidates [4–6]. The term MSCs is generally adopted to refer to miniaturized ECs that are designed and fabricated to serve as power sources or energy storage units in microelectronic devices [5]. The most common MSCs can be found in the form of in-plane interdigital patterns [7], though many stack-layer [8] and wire-shape [9] ECs also fall within the same category. The prefix micro-in the term "micro-supercapacitor" indicates a small size of the device, correspondingly the capacitance and amount of stored energy are not comparable with conventional ECs. Research efforts have been directed on improving energy density for compact energy storage. However, it is worth mentioning that the capacitance and energy level just need to be "moderate" for some applications, to limit the amount of energy loss through self-discharge and leakage current ($\propto$ energy and capacitance). The magnitude of transmitted energy by harvesters in miniaturized self-powered systems is usually relatively small, therefore the energy loss through the storage EC can be detrimental for the applications and therefore should be minimized.

Bearing in mind the high demand of cycling stability and low loss, as well as a moderate requirement of capacitance and energy for miniaturized self-powered systems, pure carbon-based electrodes can be more suitable than other composites and pseudocapacitive materials, due to relatively simple structure and composition of carbon electrodes, thus straightforward energy storage mechanism and more controllable self-discharge. Carbon-based ECs store ionic charges on the surface of the electrode, forming electrical double layers (EDL) across the electrode-electrolyte interface. The physical mechanism involves no volume expansion or contraction during charge/discharge processes [3,10]. This enables a more superior cycle life than that of pseudocapacitive mechanisms which involve a certain degree of variation in chemical states and structures and inferior lifetime [11]. Therefore, EDL storage is more suitable for "fit-and-forget" smart systems. Activated carbon has been playing a frontier role as EC electrodes due to its low cost and high surface area up to 2000 $m^2 g^{-1}$ and capacitance up to hundreds of Farads per gram of active material [12]. Activated carbon is well suited for large ECs but may exhibit significant self-discharge and leakage current, and consequently not suitable for miniature systems. This concern originates from the wide pore size distribution of activated carbon, which leads to asynchronous charging and charge redistribution effects [13]. Alternatively, low dimension carbon allotropes e.g. graphene and carbon nanotubes (CNTs) have been demonstrated for advanced ECs [14–16].

Compared with graphene, the 1D carbon material CNTs, especially the vertically aligned CNTs (VACNTs), can enhance the available surface area per device footprint for the EDL storage, and thus exhibit substantially high capacitance and energy density. In contrast to randomly entangled CNT electrodes prepared by solution processes, VACNTs have relatively well-defined tube-spacing and uniform pore structure, which are beneficial for fast ions transportation. Therefore, VACNTs have been recognized as high performance EC electrodes [17–23]. Most of the demonstrated VACNTs electrodes were fabricated by chemical vapor deposition (CVD) method on a specific substrate. By growing VACNTs on the surface of aluminum (Al) foil [18,23], flexible electrodes were fabricated and potentially can be used for flexible storage ECs. However, the Al substrate may limit the electrolyte options because Al is prone to corrosion in both acidic and alkaline solutions. After VACNTs growth on silicon wafers, D. Futaba and co-workers [17] released VACNTs from the substrate after densification in liquid and obtained freestanding VACNTs electrodes. However, possibly due to the existence of an iron catalyst layer, a deviation from capacitive behavior could be observed from the presented performance, which can cause problems of serious self-discharge or leakage current. The problem concerning the catalyst layer and its negative influence on the electrochemical performance of ECs exists in other VACNTs based ECs. For the most common CVD process, a base-growth mechanism with catalyst layer residing between the grown VACNTs and the substrate prevails. This electrode structure makes it difficult to remove catalysts without damaging the integrity of the material. Moreover, the catalyst layer could impede the electrons' transportation from VACNTs to the substrate and external circuit. Alternatively, a tip-growth process ("odako growth" [24]) was demonstrated by Y. Zhu et al. [25], with a catalyst layer deposited in the order of Fe under Al_2O_3 and eventually residing on the VACNTs tips. The VACNTs were grown on single-layer graphene attached to a copper foil with a feature of covalent bonding between graphene and VACNTs. The seamless bonding leads to enhancement in conductivity and thereby power density of the demonstrated ECs. Later, a similar structure was implemented for interdigital patterned MSCs, for AC line filtering applications [26]. The catalysts were not eliminated in either case, potentially jeopardizing the self-discharge and leakage current. Recently, tip-growth VACNTs were successfully grown on highly-oriented graphite films [27]. Covalent bonding between VACNTs and the surface graphene-like layer of the graphite substrate was achieved, enabling faster electron transportation compared to entangled CNTs electrodes or non-anchored VACNTs. The tip-growth mechanism leaves the Fe/Al_2O_3 on the tips of VACNTs, making it possible to be removed by a mild plasma treatment. Correspondingly, the graphite/VACNTs based ECs displayed excellent frequency response with high capacitance. Moreover, due to a reduced amount of catalysts, the self-discharge rate and leakage current were kept at low levels. These merits of tip-growth VACNTs on graphite make the material suitable for compact and low loss EC storage units in miniaturized self-powered systems [27]. Nevertheless, the working voltage of the demonstrated device was as low as 0.8 V, limited by the type of electrolyte e.g. PVA/H_3PO_4.

In general, low voltage is an inherent property of ECs and other electrochemical energy storage devices. For applications that require a higher voltage than the maximum voltage of a single device, one can connect two or more units in series. For interdigital patterned MSCs, MSC arrays [28,29] can be designed to achieve high operating voltage. However, the array design inevitably increases the device footprint area, which is usually very limited in miniaturized systems. In contrast, stack structured ECs in a bipolar design can achieve high voltage without enlarging footprint but only expand the volume in an efficient way. Compared with a normal series connection of multiple devices, a bipolar EC design can guarantee a higher space-efficiency and therefore higher energy density per volume of a device which is essential for miniature systems due to a limitation in space allocated for energy storage units.

In principle, a bipolar design is simply the stacking of devices through bipolar electrode plates. A bipolar electrode plate can serve as a current collector for a positive electrode in one cell, while as a negative electrode's current collector in the adjacent cell. In this way, only N+1 plates are needed for stacking N devices, while normal stacking requires 2 N plates together with 2 N individual packages. A lighter and more compact bipolar plate would further strengthen the advantage in specific and volumetric energy densities. Meanwhile, the bipolar plate should be resistant to corrosion in a wide range of electrolytes and remain highly conductive to reduce series resistance. Previous reports showed the use of titanium [30,31], stainless steel [32] and aluminum [33] as bipolar plates. For fabricating bipolar ECs, it is critical to ensure a capacitance balancing for unit devices. In an ideal case, the unit cells should be identical. Otherwise, cell imbalance will cause a severe decrease in lifetime and other metrics e.g. self-discharge. The benchmark for an efficient design and fabrication of bipolar ECs, is not to sacrifice the performance of single unit devices in the more complex

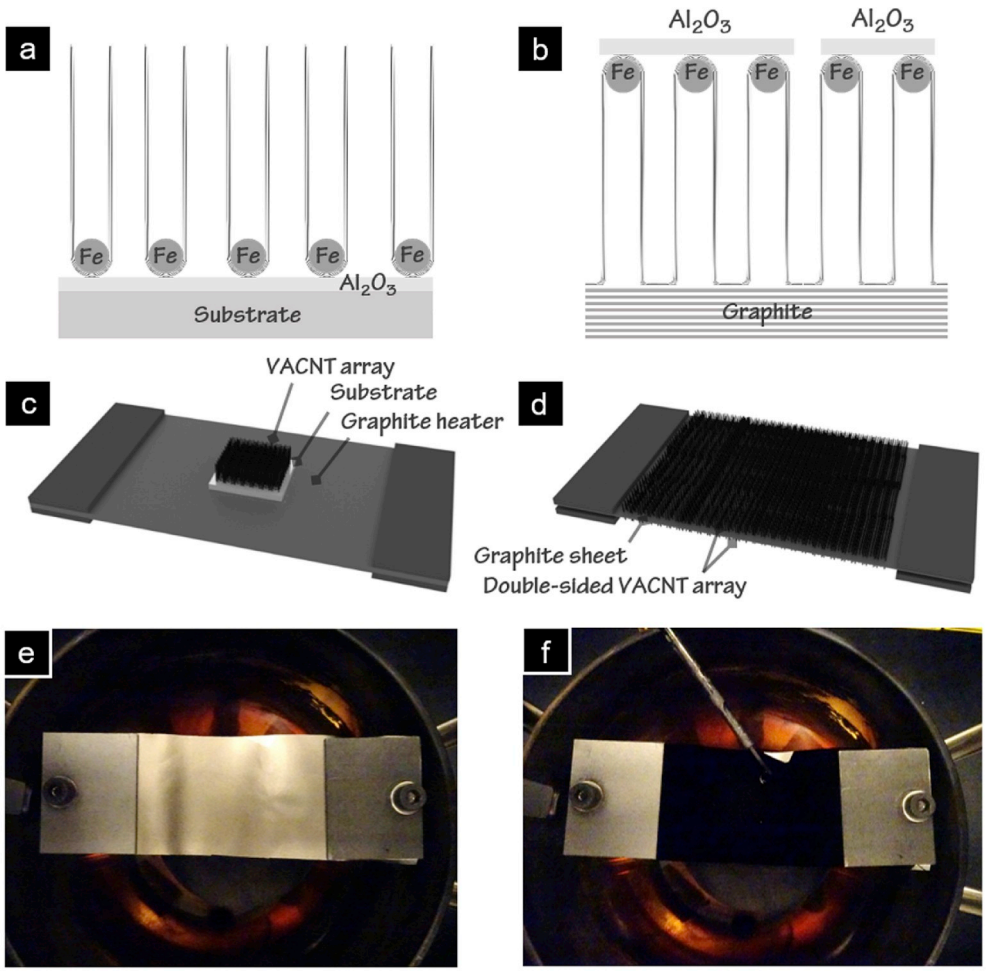

Fig. 1. a) Schematic of VACNTs grown using conventional CVD, with Fe catalyst and Al_2O_3 diffusion barrier layer beneath. **b)** VACNTs grown using odako-growth, with Fe and Al_2O_3 on top of the VACNT array. **c)** Conventional cold-wall VACNTs CVD setup, with VACNTs grown on a Si chip placed on a graphite heater. **d)** Joule heating CVD setup, with VACNTs grown directly on the graphite foil used as the heater. **e-f)** Photos of the experimental setup before and after VACNTs CVD growth, respectively.

bipolar fabrication procedure.

Fabrication of VACNTs based bipolar ECs has not been demonstrated. The obstacles for the demonstration are related to the difficulties in both electrode and device design and engineering. VACNTs are synthesized with CVD methods on substrates, and the choice of substrate material determines the feasibility of their use in bipolar designs. A smart design of VACNTs based bipolar ECs would be to directly use the substrate as a bipolar plate to save weight and space. Rigid and bulky wafers are not an option, not only because of a large weight and volume fraction of inactive components in the final product, but also their insulating nature rules out the stack structure design. For the use of freestanding VACNTs films [17] in bipolar ECs, it is necessary to use an additional layer as a bipolar plate, and the interface between the VACNTs and the bipolar plate must be optimized. Taking into account the factors discussed above, the substrate of VACNTs should be light, highly conductive, chemically inert and at the same time facilitate good contact with VACNTs. In this sense, graphite film is a perfect fit because of its chemical stability, and the possibility of enabling a seamless bonding structure. Additional merit is the flexibility of graphite film makes it possible to engineer devices in diverse form factors for miniature systems applications. It can thus be postulated that the above-mentioned tip-growth VACNTs on graphite with a seamless bonding structure [27] could be an excellent prototype for VACNTs bipolar ECs. To that end, VACNTs of the same quality must be grown on the other side of the graphite substrate, which is a demanding task.

The high quality tip-growth graphite/VACNTs electrodes for miniature ECs were fabricated with a cold-wall CVD system [27]. Usually, cold-wall CVD systems are equipped with a localized heater that raises the substrate temperature to initiate VACNTs growth. With the same setup, bipolar electrodes can only be fabricated by running the same process two times, in order to grow on both sides. The repeated process increases time consumption and potentially leads to non-uniformity of VACNTs quality. The non-uniformity can be caused by any difference in parameter control between the two successive runs, and also because the VACNTs grown during the first run must undergo an additional process run that involves high temperature growth conditions, the quality can thus be different from that of VACNTs grown on the other side during the second run. To eliminate the concerns, it is preferable to grow VACNTs simultaneously on both sides of the substrate. Base-growth VACNTs on both sides of copper foils were grown using conventional quartz tube furnaces [34–36] where the copper substrates were heated up by heating elements along the quartz tube. Compared with cold-wall systems, these methods pose disadvantages in terms of energy consumption, process speed, and scalability. Since graphite is both electronically and thermally conductive, a new CVD method can be developed by using the graphite substrate directly as a heating element in cold-wall systems. The current directly runs through the graphite that is heated up through the joule heating effect. The substrate temperature and ramping rate can be regulated by controlling the input power. In this way, VACNTs grow on both sides of the substrate in a single run. A double-side VACNTs on graphite material was fabricated with such a self-joule heating CVD method for thermal applications [37]. However, the VACNTs growth was based on base-growth mechanism, therefore lacking the advantages of seamless bonding structure and ease of catalyst removal, and it cannot be directly used as EC electrodes for miniature systems that require low loss.

In this work, we are dedicated to developing a new process for fabricating tip-growth VACNTs on both sides of highly oriented graphite

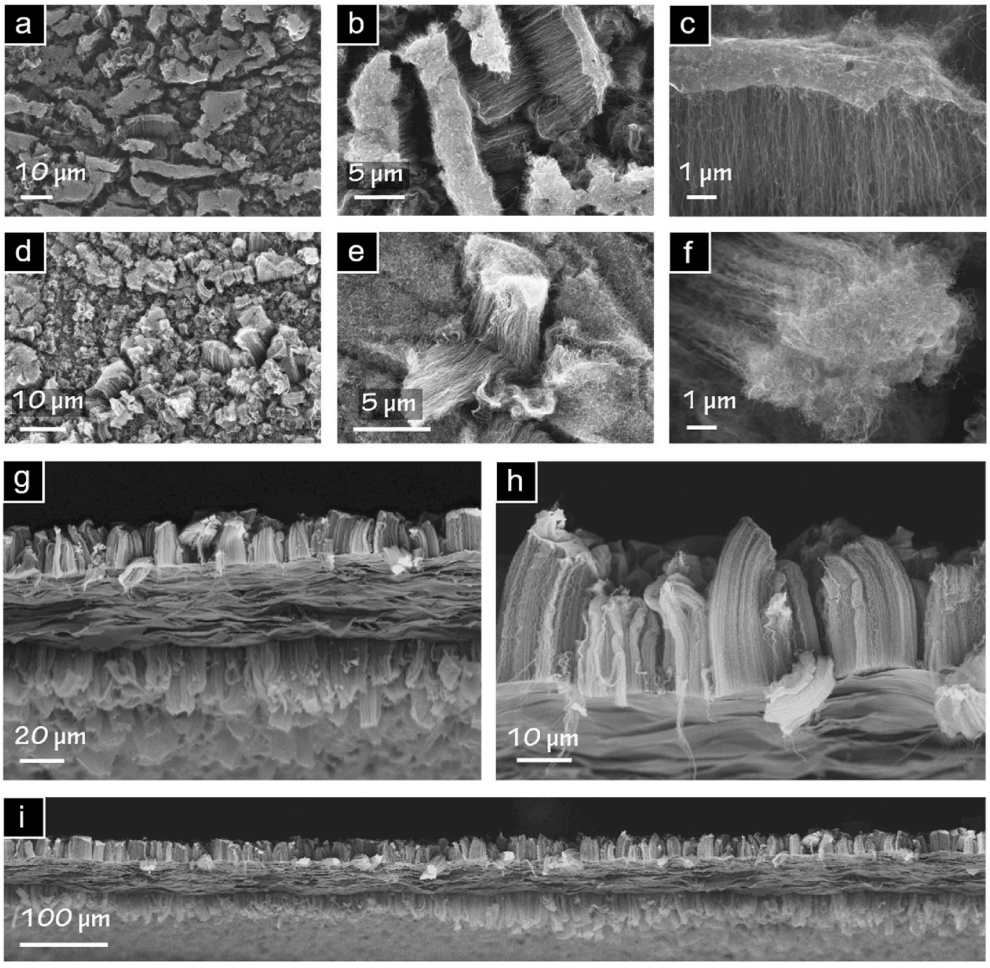

Fig. 2. SEM images of the VACNT arrays grown on both sides of a graphite foil. **a)** The as-grown VACNT arrays are broken up into segments with an intact alumina layer on top. **b)** Higher magnification of VACNT arrays. **c)** Magnification of a single VACNT bundle caused by one alumina sheet. **d-f)** Corresponding images of VACNT arrays after plasma etching and the removal of alumina. **g)** Side view of the double-sided graphite/VACNTs hybrid material. **h)** Magnification of the VACNT arrays from the side. **i)** Zoomed out view of the double-sided graphite/VACNTs hybrid.

films, and demonstrate the first VACNTs based miniature bipolar ECs. With an energy-saving, fast and scalable self-joule heating CVD method, VACNTs were grown on both sides of the graphite substrate in one process run, with the feature of tip-growth and excellent contact to the substrate. After a plasma treatment to remove the catalyst layer, the materials were used for bipolar ECs of an efficient design. The demonstrated bipolar ECs exhibited non-impaired performance compared with single units. The presented electrode and fabrication strategy provide hints for developing advanced ECs for miniaturized self-powered systems.

2. Double-sided graphite/VACNT (DSGC) bipolar electrodes

Conventional VACNTs CVD utilizes a catalyst structure consisting of a ceramic barrier layer with a metal catalyst layer on top. Fig. 1a shows the structure of an array of VACNTs synthesized this way. During the CVD process, VACNTs grow upward from the metal particles, which are immobilized by the ceramic layer [38]. However, this leaves the catalysts at the interface between each VACNTs and the underlying substrate, most notably the ceramic layer which aggravates self-discharge and prevents a good electrical connection which is crucial for EC applications.

In order to form a seamless connection between the VACNTs and the underlying carbon substrate, so-called “odako” growth can be used. By reversing the catalyst layer structure, and depositing Fe catalyst underneath an alumina layer, the catalyst stays on top of the VACNTs array, forming bundles of VACNTs with alumina flakes on top [24], as shown in Fig. 1b. This method can form a seamless, covalent bonding between the VACNTs and the topmost graphene layer [25,39] and has previously been demonstrated as a good candidate for EC electrode material [27].

The double-sided graphite/VACNTs (DSGC) bipolar electrode material was fabricated through a recently developed joule heating CVD method [37]. The method is based on a cold-wall CVD system, where the substrate for VACNTs synthesis is placed on a graphite heater in a low pressure chamber, as seen in Fig. 1c. However, rather than placing the chip on a heater, a 25 μm thick pyrolytic graphite sheet (PGS) from Panasonic was used as both substrate and heater, enabling growth on a larger area and simultaneously on both sides of the substrate. In principle, PGS can be thinned down mechanically through e.g. scotch tape method [40].

The catalyst layer consisted of 2 nm Fe and 3 nm Al_2O_3, consecutively deposited by an electron beam evaporator (AVAC HVC600). The VACNTs CVD setup is shown schematically in Fig. 1d. The graphite foil was fastened between two electrodes inside the reaction chamber. The process took place at a low pressure in a vacuum chamber with a gas inlet for reactant gases. The sample was heated by joule heating from an applied current through the graphite sheet, regulated with a thermocouple in contact with the substrate. The temperature was ramped up to 500 °C at a rate of 300 °C/min with a flow of 837 sccm of H_2, and subsequently held stable for 3 min for reduction of catalyst and cracking of the alumina layer. In the growth step, the temperature was then quickly ramped up to 650 °C and a flow of 240 sccm C_2H_2 for 10 min was introduced into the chamber. Fig. 1e and f shows the CVD setup before and after the growth of a DSGC. VACNTs have grown on the entire area between the electrodes.

Besides DSGC, we fabricated another version of EC electrodes: single-sided graphite/VACNTs (SSGC) to be used as end electrodes in bipolar

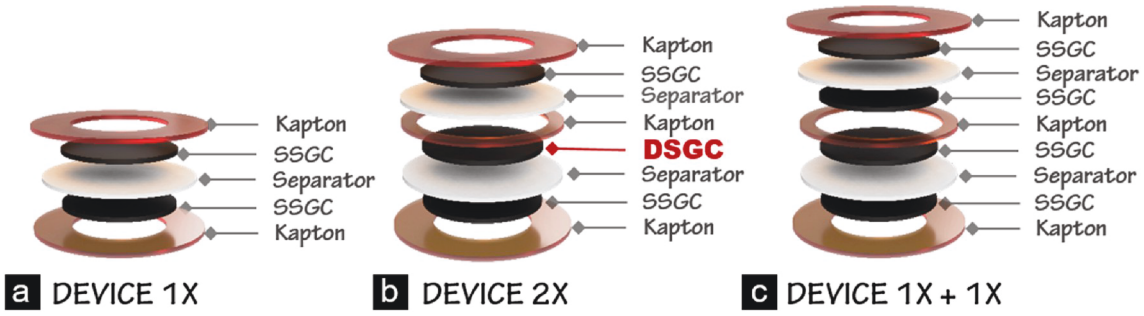

Fig. 3. Schematics of devices **a)** 1 × , **b)** 2 × and **c)** 1 × + 1×

designs. SSGC were fabricated by catalyst deposition on only one side, while the DSGC required sequential catalyst deposition on both sides.

Scanning electron microscope (SEM) images of the fabricated VACNT arrays are presented in Fig. 2. Fig. 2a–c show the as-grown VACNT arrays. During growth, the alumina layer is cracked into flakes, each of which rests on top of a VACNT bundle. Each of these bundles are held together by the alumina, which stays on top of the array, but are relatively independent from each other. The end result is that the VACNT array consists of bundles with slight different height and orientation, seen clearly in Fig. 2h.

Samples were subjected to post-growth O_2 plasma treatment at 100 W for 30 s in order to remove the alumina from the top of the VACNT arrays. Fig. 2d–f show the VACNT arrays post plasma etching, as compared to Fig. 2a–c respectively. Before plasma etching, the alumina flakes were clearly defined, while almost completely absent after treatment, with exposed VACNT tips visible instead.

Fig. 2g shows a side view of the DSGC, with a closer view of the side of the VACNT arrays in Fig. 2h. Individual VACNT bundles vary in length, but the average VACNT array height is approximately 30 m, with a total thickness of the graphite/VACNTs hybrid of 85 m. The height was chosen to optimize the trade-off between longer CNTs and array uniformity, where longer CNTs growth time causes unacceptable variation in height between bundles. This variation is typical of odako-growth of VACNT arrays, and the arrays in this work have similar height and uniformity as previously reported comparable CNTs arrays on graphite [24,27]. On a larger scale, as seen in Fig. 2i, the uniformity of the VACNT arrays is still relatively even.

Gravimetric measurements showed a weight fraction of 6% VACNTs for the DSGC sample, corresponding to about 3% for each side. The VACNT arrays were further characterized by XPS and Raman measurements which can be found in the supplementary information. The results are consistent with previous works despite the modification of the CVD process. However, the relatively high defect concentration of the VACNTs leaves a potential for significant further improvements.

3. Bipolar electrochemical capacitors

3.1. Device fabrication

Three different types of EC devices were fabricated for comparison.

The first type, denoted as "1 × ", is in a normal quasi-solid stack configuration with SSGC as the electrode materials. A schematic in Fig. 3a demonstrates the device structure. The fabrication started with a piece of SSGC in size of dia. 8 mm placed on a Teflon substrate, with approximately 3 μL PVA/H_3PO_4 electrolyte dropped on the VACNTs side. The hydrophilicity of SSGC allows the water based gel electrolyte to spread evenly over the surface. Afterward, a piece of dia. 10 mm cellulose separator was placed on top and then wetted by the electrolyte. In the subsequent step, another piece of SSGC was used with the VACNTs side facing downwards and aligned to the first electrode. A vacuum pen was deployed to facilitate the assembly process. After drying in vacuum for 3 h at 90 °C, the material stack was separated from the Teflon substrate, and encapsulated under compression by Kapton tape O-rings with outer dia. 12 mm and inner dia. 6 mm. The total thickness of device 1x was measured to be about 70 μm.

The second type of device, denoted as "2 × ", is the bipolar quasi-solid EC with one layer of DSGC material. A schematic in Fig. 3b demonstrates the device structure. The fabrication also started with a piece of SSGC electrode and 3 μL PVA/H_3PO_4 electrolyte followed by cellulose separator. Instead of a piece of SSGC for 1 × device fabrication, DSGC was applied on the top. After drying in the same conditions, a piece of Kapton O-ring tape (outer dia. 12 mm and inner dia. 8 mm) was aligned and glued to the separator periphery, for preventing from electrolyte crossover between adjacent unit cells. Then, the application of electrolyte, separator was repeated carefully, and finally capped with a piece of SSGC end electrode before drying. The device was encapsulated by Kapton tape O-rings. The total thickness of device 2 × was measured to be approximately 115 μm.

The third type of device, denoted as "1 × + 1 × " (Fig. 3c), is a stack of two 1 × devices, equivalent to two SSGCs back-to-back replacing the DSGC bipolar electrode in device 2 ×. Device 1 × + 1 × is a representative of a series connection of EC units. The total thickness of device 1 × + 1 × was measured to be about 140 m.

3.2. Electrochemical characterization methods

Electrochemical characterizations were conducted with Gamry Reference 3000 AE potentiostat. Cyclic voltammograms (CV), galvanostatic charge/discharge (GCD), electrochemical impedance spectroscopy (EIS) and cyclic charge/discharge (CCD), as well as self-discharge measurements, were applied to fully evaluate the device performances. Device areal capacitance (mF cm^{-2}) was calculated from GCD measurements through the equation

$$C_A = 1000 \times \frac{I \times t}{V_{max} - V_{IR}} \quad (1)$$

where I (A cm^{-2}) is the current density calculated based on the device area A, t (s) is the discharge time, and VIR (V) is the IR drop. The factor 1000 converts the unit of capacitance from F to mF.

Areal energy density (μWh cm^{-2}) and areal power density (μW cm^{-2}) were calculated according to

$$E_A = 1000 \times \frac{C_A \times (V_{max} - V_{IR})^2}{2 \times 3600} \quad (2)$$

$$P_A = \frac{3600 \times E_A}{t} \quad (3)$$

The factors 1000 and 3600 in Equations (2) and (3) converts the units from mWh to μWh, and seconds to hours, respectively. Volumetric capacitance (C_V, F cm^{-3}), energy (E_V, μWh cm^{-3}) and power (P_V, μW cm^{-3}) can be obtained through dividing C_A, E_A and P_A values by the device thickness values.

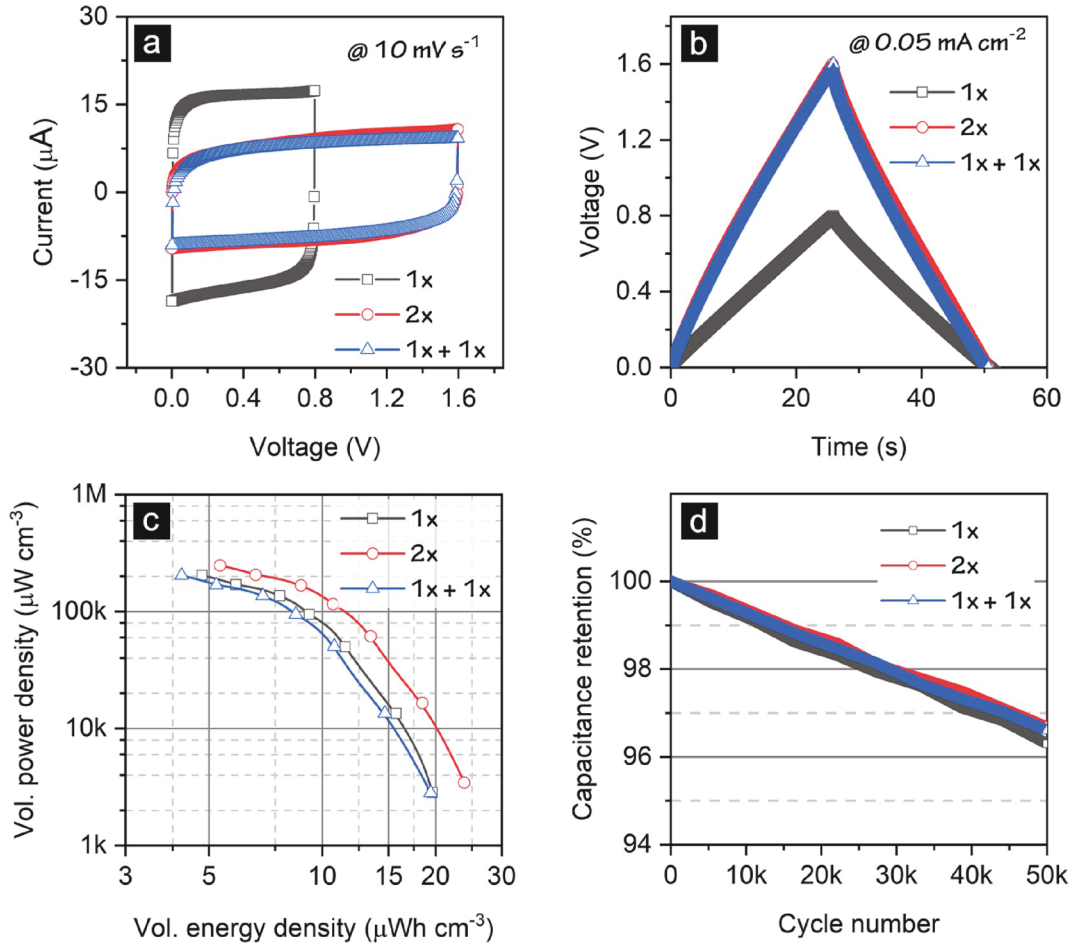

Fig. 4. Performance of devices 1 × , 2 × and 1 × + 1 × . **a)** CV scans and **b)** GCD curves within respective voltage ranges; **c)** Ragone plot; **d)** Cycling stability.

Table 1
Performance metrics of devices 1 × , 2 × and 1 × + 1×

Device	areal vol.	Capacitance (mF cm^{-2}) (F cm^{-3})	Energy (μWh cm^{-2}) (μWh cm^{-3})	Power (μW cm^{-2}) (μW cm^{-3})	Voltage (V)	Rate capability	Cycling stability
1 ×		1.57	0.14	19.83	0.8	47%	96.3%
		0.22	19.61	2832.14			
2 ×		0.78	0.27	39.73	1.6	44%	96.7%
		0.068	23.85	3454.35			
1 × + 1 ×		0.78	0.27	39.50	1.6	42%	96.6%
		0.056	19.40	2821.43			

3.3. Electrochemical performances

Electrochemical performances of device 1 ×, 2 × and 1 × + 1 × are displayed in Fig. 4 and Table 1. Fig. 4a represents CV curves at a scan rate of 10 mV s^{-1} of the three devices within respective voltage ranges. The quasi-rectangular curves demonstrate the dominance of the EDL storage mechanism. At the same scan rate, device 1 × exhibited current response approximately two times of device 1 × + 1 ×, corresponding to two folds of capacitance. The result complies the relation of capacitor series connection, i.e.

$$\frac{1}{C_{1\times+1\times}} = \frac{1}{C_{1\times}} + \frac{1}{C_{1\times}} \quad (4)$$

The decreased capacitance of the stack devices was compensated by the two fold increase in voltage window from 0.8 V to 1.6 V. The amount of energy per sub-cell remained the same, and devices 2 × and 1 × + 1 × have approximately 2 times the energy of device 1 ×.

Device 2 × displayed almost the same current response and thus similar capacitance as for device 1 × + 1 ×, suggesting that each VACNTs layer in device 2x resembled those in device 1 ×. This feature is of significance for engineering bipolar devices. Each pair of electrodes in bipolar devices should have rather similar capacitance values for cell balancing, and avoiding overcharging/discharging any individual unit components; otherwise, electrolyte decomposition, electrode oxidation and eventually accelerated device aging is inevitable [41].

In accordance to CV results, the GCD measurements in Fig. 4b show almost overlapped linear curves for device 2 × and 1 × + 1 × at voltage window 1.6 V, while device 1 × displayed triangle GCD curves within 0.8 V. All devices were fully charged and discharged in nearly the same time periods, which is another proof of reproducibility of electrode quality with a joule heating method.

As mentioned earlier and manifested by CV and GCD results, the energy values are close to each other for the device 2 × and 1 × + 1 ×, however, when normalized to the total device volumes, differences

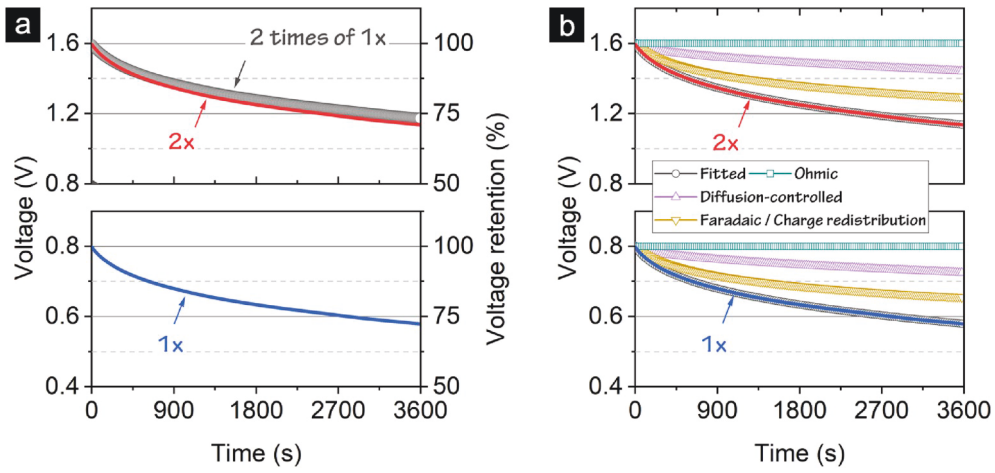

Fig. 5. Comparison of self-discharge between devices 1 × and 2 × . **a**) Original data and **b**) curve fitting.

become significant. The boost in volume-, as well as weight-based metrics is a clear advantage of bipolar designs, because of the less usage of current collector (graphite paper in this work) and packaging materials. As shown in Fig. 4c, the bipolar device 2 × has about a 22% increase in volumetric energy density and power density, reaching 23.85 μWh cm^{-3} and 3454.35 μW cm^{-3}. Moreover, another advantage of bipolar 2 × device is potentially reduced equivalent series resistance (ESR) compared to device 1 × + 1 ×. Although marginal difference in ESR can be observed here in the case of 2 × and 1 × + 1 ×, the ESR of connecting multiple 1 × devices can surge to a huge value, providing one imperfect connection would occur between any of two adjacent cells. In contrast, adjacent cells are connected seamlessly through one piece of graphite current collector in the DSGC based bipolar design, thus enabling reducing the ESR from contacts, besides simplifying the fabrication process.

The enhancement in energy and power was achieved at no sacrifice of cycling stability as shown in Fig. 4d. Capacitance retention of 96.7% was found over 50 000 cycles of charge/discharge process, obviously indicating the absence, or fairly insignificant if any, of cell imbalance. Together with the overlapping curves, this is another indication of the uniformity of VACNTs growth.

Self-discharge has been recognized as one of the most problematic features of ECs [42–44], especially for applications in miniaturized systems where the power source is limited. Fig. 5a shows the comparison of self-discharge properties of device 1 × and 2 ×. For the convenience of quantifying, the data is presented in two separate panels for different working voltage windows. After 1 h of open circuit from the respective fully charged state, device 1 × and 2 × retained 72.6% and 71.2% of original voltage. By mathematically scaling the self-discharge curve of device 1 × by multiplying each data point by a factor of 2, it can be seen that the actual 2x device voltage decay generally followed the projected curve. These results indicate that the self-discharge process was not aggravated by the graphite/VACNTs bipolar designs.

To further elucidate the involved self-discharge mechanisms, curve fitting was performed on both devices. It is generally acknowledged that mechanisms following three different voltage-time function forms are involved [42,45]. One is ohmic leakage mechanism caused by any imperfect insulating components, voltage curve is presented as

$$V = V_0 \exp\left(-\frac{t}{a}\right) \tag{5}$$

where a is the time constant of the capacitor. The second is a diffusion-controlled mechanism, caused by a low concentration of impurity ions shuttling between electrodes, following the equation

$$V = V_0 - b\sqrt{t} \tag{6}$$

where b is a product of values including diffusion constants. The third class of mechanisms is divided into activation-controlled discharge and charge-redistribution. The former is related to overcharging to potentials above the thermodynamic equilibrium values of redox reactions (from impurities). The latter is a dynamic equilibrium process due to the non-uniformity of pore sizes in porous electrodes. Voltage decay caused by both mechanisms mathematically follows the same trend

$$V = V_0 - c - d\ln(t + e) \tag{7}$$

where c, d and e are constants varying from system to system. Combining all the mechanisms, the self-discharge curve can thus be modelled as

$$V = V_0 \exp\left(-\frac{t}{a}\right) - b\sqrt{t} - c - d\ln(t + e) \tag{8}$$

Curve fitting using the above model intends to deconvolute the self-discharge curves into the three terms representing different mechanisms, as shown in Fig. 5b. Note that only by assuming zero contribution from ohmic leakage can a reasonable fitting be performed. This is in accordance with a recent work where it is explained by ideal insulation between electrodes and encapsulation [46]. According to the result, the diffusion-controlled process accounts for 22.8% voltage loss, and the rest results from Faradaic activation-controlled or charge redistribution mechanisms. As the vertically aligned CNTs render relatively uniform structures, charge redistribution is regarded as a minor issue herein. The

Table 2
Volumetric performance comparison of CNT based ECs.

Material (device)	Electrolyte	Voltage (V)	Vol. capacitance (F cm^{-3})	Vol. energy (Wh cm^{-3})	Vol. power (μW cm^{-3})	Ref.
DSGC (2 ×)	PVA/H_3PO_4	1.6	0.068	23.85	3454.35	This work
SSGC (1 ×)	PVA/H_3PO_4	0.8	0.22	19.61	2832.14	
Paper/CNTs	PVA/H_2SO_4	1.0	0.004	0.52	186.57	[47]
PET/CNTs	PVA/H_3PO_4	1.0	0.014	1.81	211.11	[48]
Al/CNTs	Na_2SO_4	0.8	0.089	7.9	1333.33	[49]
Graphene/CNTs	H_2SO_4	0.8	0.022	6.97	313.44	[50]

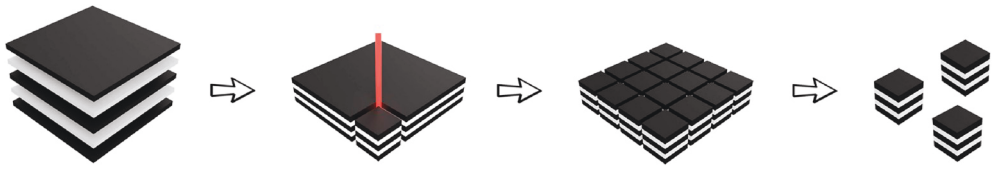

Fig. 6. Schematic of device fabrication by laser cutting.

presence of residual catalyst particles, especially Fe that can lead to Fe^{3+}/Fe^{2+} shuttle ions and redox reactions may be the major cause of self-discharge. Nevertheless, the capacitance retention over 1 h with only a short voltage holding period is satisfactory, meaning the residual content is relatively low, as suggested by the XPS spectrum in supporting information (Fig. S1).

4. Discussion

Table 2 shows a comparison of the volumetric performance of CNT based ECs. As can be seen, the graphite/VACNTs based ECs display state-of-art performance at a device level in comparison to previously reported CNT based devices, owing largely to the seamless bonding between surface graphite and VACNT arrays generated during CVD growth [25,27,39]. This unique bonding feature could enable a relatively high loading of long VACNTs thus high energy density with little compromise in power densities [27].

With the new self-joule heating CVD method, sufficient uniformity of the VACNT arrays was achieved to allow for bipolar electrode stacking. We have demonstrated a prototype device 2 × with stacking one layer of DSGC bipolar electrode, improving approximately 22% volumetric energy compared to a series connection of 1 × devices, reaching 23.85 μWh cm^{-3}. This already significant improvement of the volumetric metrics can be further enhanced by stacking more layers of bipolar electrodes. According to the thickness values of device 2 × (115 μm) and 1 × (70 μm), the thickness of device "N × " is 70 + 45 × (N - 1) μm. Assuming a linear relationship between energy value (Wh) and the number of unit cells (N), the percentage of volumetric energy increase compared to a series connection of a number of N 1 × devices is

$$\left[\frac{70 \times N}{70 + 45 \times (N-1)} - 1\right] \times 100\% \quad (9)$$

According to the relationship, a relatively rapid increase of volumetric energy can be envisaged by increasing N from 2 to 10 approaching a limit of 55% improvement over a series connection of 1 × devices. Further stacking results in a slower increase in energy but a continuous linear increase in operating voltage.

Fabrication of bipolar ECs with multiple bipolar electrodes can be a complicated process for demonstrating lab-scale prototypes through manual assembly, due to the special attention to ensure precise electrode alignment and to avoid electrolyte crossover. Nevertheless, we have demonstrated a prototype fabrication that improves voltage limit and energy density at no expenses in cycling stability and self-discharge, benchmarking a rational bipolar design with the unique DSGC material. The difficulty associated with manual handling in fabrication could be combated in the mass production process, with the aid of automatized machines. Fig. 6 illustrates a possible solution for up-scale production of DSGC based bipolar ECs. The electrode and separator/electrolyte stack wafers are prepared first (alignment is more convenient to be done when handling a large piece of materials), after which bipolar devices of arbitrary lateral dimensions can be individualized through dicing the wafers with a dicing saw or a laser cutter. Finally, the diced units can be encapsulated individually. Combining this method with the developed joule heating CVD for DSGC materials, a comparatively simple and highly scalable method, enables mass production of inexpensive high-performance ECs.

Similar methods could be used to create high voltage AC line filters using an aqueous electrolyte instead, although a higher degree of difficulty is inevitable in preventing electrolyte crossover. The double-sided graphite/VACNTs can also simply serve as 3D current collectors and bipolar plates for constructing more advanced bipolar ECs. Finally, the graphite/VACNTs material can be useful for other applications utilizing VACNT array properties and strong bonding towards graphite, for instance, thermal interface materials or heat spreaders.

5. Conclusions

This work demonstrates bipolar electrochemical capacitors featuring double-sided VACNTs on graphite electrodes, which is obtained by a novel joule heating CVD method. The bipolar device exhibited a 22% increase in volumetric energy comparing to a series connection of two unit devices. The energy value reaching 23.85 μWh cm^{-3} at a device level represents the state-of-art CNTs based ECs. The voltage decay of bipolar devices over a self-discharge process was kept as low as its unit cells. A 71% voltage is retained after 1 h open-circuit after charging to 1.6 V and only 5 min voltage hold. The capacitance retention is as high as 96.7% after 50 000 cycles, proving the absence of cell imbalance and high uniformity of electrodes. This works serves as a proof of concept for the stacking of bipolar graphite/VACNTs for ECs, with significant additional performance enhancement envisioned for further stacking of additional layers within one device. In addition, the fabrication methods are compatible with large-scale simultaneous fabrication of multiple devices, allowing for the possibility of industrial utilization of VACNTs based bipolar ECs for miniaturized self-powered systems.

Declaration of competing interest

The authors declare that they have no known competing financial interests or personal relationships that could have appeared to influence the work reported in this paper.

Acknowledgements

This research was funded by the Swedish National Science Foundation with the contract No: 621-2007-4660, by the Swedish Board for Innovation (Vinnova) within the Siografen Program, by the Swedish Board for Strategic Research (SSF) with the contract No: SE13-0061 and by Formas with the contract No: FR-2017/0009 and by the Production Area of Advance at Chalmers University of Technology, Sweden, by the VINNOVA UDI project No. 2017–03725 Energy Supply Toolkit, by the VINNOVA NFFP7 project No. 2017–04869 Architecture for High-Power Radars. The research was also partially supported by the National Science Foundation (NSF) through the Materials Research Science and Engineering Center at UC Santa Barbara, DMR-1720256 (Internship to Chalmers University of Technology).

Appendix A. Supplementary data

Supplementary data to this article can be found online at https://doi.org/10.1016/j.jpowsour.2020.227765.

References

[1] Energy Autonomy in IoT Technologies, Energy Procedia 156, 2019, pp. 222–226, https://doi.org/10.1016/J.EGYPRO.2018.11.132. https://www.sciencedirect.com/science/article/pii/S1876610218310920.

[2] S. Sudevalayam, P. Kulkarni, Energy harvesting sensor nodes: survey and implications, IEEE Communications Surveys & Tutorials 13 (2010) 443–461.

[3] P. Simon, Y. Gogotsi, Materials for electrochemical capacitors, Nat. Mater. 7 (2008) 845, https://doi.org/10.1038/nmat2297.

[4] N.A. Kyerematen, T. Brousse, D. Pech, Microsupercapacitors as miniaturized energy-storage components for on-chip electronics, Nat. Nanotechnol. 12 (2017) 7–15, https://doi.org/10.1038/nnano.2016.196. https://www.ncbi.nlm.nih.gov/pubmed/27819693.

[5] M. Beidaghi, Y. Gogotsi, Capacitive energy storage in micro-scale devices: recent advances in design and fabrication of micro-supercapacitors, Energy Environ. Sci. 7 (2014) 867–884, https://doi.org/10.1039/c3ee43526a.

[6] H. Zhang, Y. Cao, M.O.L. Chee, P. Dong, M. Ye, J. Shen, Recent advances in micro-supercapacitors, Nanoscale 11 (2019) 5807–5821, https://doi.org/10.1039/c9nr01090d. https://www.ncbi.nlm.nih.gov/pubmed/30869718.

[7] J. Chmiola, C. Largeot, P.L. Taberna, P. Simon, Y. Gogotsi, Monolithic carbide-derived carbon films for micro-supercapacitors, Science 328 (2010) 480–483, https://doi.org/10.1126/science.1184126. https://www.ncbi.nlm.nih.gov/pubmed/20413497.

[8] H.-K. Kim, S.-H. Cho, Y.-W. Ok, T.-Y. Seong, Y. S. Yoon, All solid-state rechargeable thin-film microsupercapacitor fabricated with tungsten cosputtered ruthenium oxide electrodes, J. Vac. Sci. Technol. B: Microelectronics and Nanometer Structures Processing, Measurement, and Phenomena 21 (????) 949–952. doi: 10.1116/1.1565348.

[9] Z. Cai, L. Li, J. Ren, L. Qiu, H. Lin, H. Peng, Flexible, weavable and efficient microsupercapacitor wires based on polyaniline composite fibers incorporated with aligned carbon nanotubes, J. Mater. Chem. 1 (2013) 258–261, https://doi.org/10.1039/c2ta00274d.

[10] M. Inagaki, H. Konno, O. Tanaike, Carbon materials for electrochemical capacitors, J. Power Sources 195 (2010) 7880–7903.

[11] M.R. Lukatskaya, B. Dunn, Y. Gogotsi, Multidimensional materials and device architectures for future hybrid energy storage, Nat. Commun. 7 (2016) 12647, https://doi.org/10.1038/ncomms12647.

[12] P. Simon, Y. Gogotsi, Capacitive energy storage in nanostructured carbon–electrolyte systems, Accounts of chemical research 46 (2012) 1094–1103, https://doi.org/10.1021/ar200306b.

[13] S. Fletcher, V.J. Black, I. Kirkpatrick, A universal equivalent circuit for carbon-based supercapacitors, J. Solid State Electrochem. 18 (2014) 1377–1387, https://doi.org/10.1007/s10008-013-2328-4.

[14] Z.-S. Wu, Y.-Z. Tan, S. Zheng, S. Wang, K. Parvez, J. Qin, X. Shi, C. Sun, X. Bao, X. Feng, et al., Bottom-up fabrication of sulfur-doped graphene films derived from sulfur-annulated nanographene for ultrahigh volumetric capacitance micro-supercapacitors, J. Am. Chem. Soc. 139 (2017) 4506–4512, https://doi.org/10.1021/jacs.7b00805.

[15] N. Islam, M.N.F. Hoque, W. Li, S. Wang, J. Warzywoda, Z. Fan, Vertically edge-oriented graphene on plasma pyrolyzed cellulose fibers and demonstration of kilohertz high-frequency filtering electrical double layer capacitors, Carbon 141 (2019) 523–530, https://doi.org/10.1016/j.carbon.2018.10.012.

[16] Y. Yoo, S. Kim, B. Kim, W. Kim, 2.5 v compact supercapacitors based on ultrathin carbon nanotube films for ac line filtering, J. Mater. Chem. 3 (2015) 11801–11806, https://doi.org/10.1039/C5TA02073E.

[17] D.N. Futaba, K. Hata, T. Yamada, T. Hiraoka, Y. Hayamizu, Y. Kakudate, O. Tanaike, H. Hatori, M. Yumura, S. Iijima, Shape-engineerable and highly densely packed single-walled carbon nanotubes and their application as super-capacitor electrodes, Nat. Mater. 5 (2006) 987–994, https://doi.org/10.1038/nmat1782. https://www.ncbi.nlm.nih.gov/pubmed/17128258.

[18] R. Reit, J. Nguyen, W.J. Ready, Growth time performance dependence of vertically aligned carbon nanotube supercapacitors grown on aluminum substrates, Electrochim. Acta 91 (2013) 96–100, https://doi.org/10.1016/j.electacta.2012.12.058.

[19] B. Hsia, J. Marschewski, S. Wang, J.B. In, C. Carraro, D. Poulikakos, C. P. Grigoropoulos, R. Maboudian, Highly flexible, all solid-state micro-supercapacitors from vertically aligned carbon nanotubes, Nanotechnology 25 (2014), 055401, https://doi.org/10.1088/0957-4484/25/5/055401. https://www.ncbi.nlm.nih.gov/pubmed/24407158.

[20] C. Zhang, Z. Peng, J. Lin, Y. Zhu, G. Ruan, C.-C. Hwang, W. Lu, R.H. Hauge, J. M. Tour, Splitting of a vertical multiwalled carbon nanotube carpet to a graphene nanoribbon carpet and its use in supercapacitors, ACS Nano 7 (2013) 5151–5159.

[21] M.G. Hahm, A. Leela Mohana Reddy, D.P. Cole, M. Rivera, J.A. Vento, J. Nam, H. Y. Jung, Y.L. Kim, N.T. Narayanan, D.P. Hashim, C. Galande, Y.J. Jung, M. Bundy, S. Karna, P.M. Ajayan, R. Vajtai, Carbon nanotube-nanocup hybrid structures for high power supercapacitor applications, Nano Lett. 12 (2012) 5616–5621, https://doi.org/10.1021/nl3027372. https://www.ncbi.nlm.nih.gov/pubmed/23030825.

[22] A. Ghosh, V.T. Le, J.J. Bae, Y.H. Lee, Tlm-psd model for optimization of energy and power density of vertically aligned carbon nanotube supercapacitor, Sci. Rep. 3 (2013) 2939, https://doi.org/10.1038/srep02939. https://www.ncbi.nlm.nih.gov/pubmed/24145831.

[23] I.B. Dogru, M.B. Durukan, O. Turel, H.E. Unalan, Flexible supercapacitor electrodes with vertically aligned carbon nanotubes grown on aluminum foils, Progress in Natural Science-Materials International 26 (2016) 232–236, https://doi.org/10.1016/j.pnsc.2016.05.011. <Go to ISI>://WOS:000380692000004.

[24] C.L. Pint, N.T. Alvarez, R.H. Hauge, Odako growth of dense arrays of single-walled carbon nanotubes attached to carbon surfaces, Nano Research 2 (2009) 526–534, https://doi.org/10.1007/s12274-009-9050-7. http://link.springer.com/10.1007/s12274-009-9050-7.

[25] Y. Zhu, L. Li, C. Zhang, G. Casillas, Z. Sun, Z. Yan, G. Ruan, Z. Peng, A.-R.O. Raji, C. Kittrell, et al., A seamless three-dimensional carbon nanotube graphene hybrid material, Nat. Commun. 3 (2012) 1225, https://doi.org/10.1038/ncomms2234. http://www.nature.com/articles/ncomms2234.

[26] J. Lin, C. Zhang, Z. Yan, Y. Zhu, Z. Peng, R.H. Hauge, D. Natelson, J.M. Tour, 3-dimensional graphene carbon nanotube carpet-based microsupercapacitors with high electrochemical performance, Nano Lett. 13 (2013) 72–78, https://doi.org/10.1021/nl3034976. https://www.ncbi.nlm.nih.gov/pubmed/23237453.

[27] Q. Li, S. Sun, A.D. Smith, P. Lundgren, Y. Fu, P. Su, T. Xu, L. Ye, L. Sun, J. Liu, P. Enoksson, Compact and low loss electrochemical capacitors using a graphite/carbon nanotube hybrid material for miniaturized systems, J. Power Sources 412 (2019) 374–383, https://doi.org/10.1016/J.JPOWSOUR.2018.11.052. https://www.sciencedirect.com/science/article/abs/pii/S0378775318312990.

[28] S.Y. Hong, J. Yoon, S.W. Jin, Y. Lim, S.-J. Lee, G. Zi, J.S. Ha, High-density, stretchable, all-solid-state microsupercapacitor arrays, ACS Nano 8 (2014) 8844–8855, https://doi.org/10.1021/nn503799j.

[29] K.U. Laszczyk, K. Kobashi, S. Sakurai, A. Sekiguchi, D.N. Futaba, T. Yamada, K. Hata, Lithographically integrated microsupercapacitors for compact, high performance, and designable energy circuits, Advanced Energy Materials 5 (2015) 1500741, https://doi.org/10.1002/aenm.201500741. <Go to ISI>://WOS:000362161500007.

[30] X. Zhou, C. Peng, G.Z. Chen, 20 v stack of aqueous supercapacitors with carbon (-), titanium bipolar plates and cnt-polypyrrole composite (+), AIChE J. 58 (2012) 974–983, https://doi.org/10.1002/aic.12632.

[31] X. Liu, T. Wu, Z. Dai, K. Tao, Y. Shi, C. Peng, X. Zhou, G.Z. Chen, Bipolarly stacked electrolyser for energy and space efficient fabrication of supercapacitor electrodes, J. Power Sources 307 (2016) 208–213, https://doi.org/10.1016/j.jpowsour.2016.01.006.

[32] J.P. Zheng, Resistance distribution in electrochemical capacitors with a bipolar structure, J. Power Sources 137 (2004) 158–162, https://doi.org/10.1016/j.jpowsour.2004.05.036.

[33] T. Sato, S. Marukane, T. Morinaga, T. Kamijo, H. Arafune, Y. Tsujii, High voltage electric double layer capacitor using a novel solid-state polymer electrolyte, J. Power Sources 295 (2015) 108–116, https://doi.org/10.1016/j.jpowsour.2015.06.116.

[34] Huan Wang, Jiyun Feng, K.M. Xijun Hu, Ng*, synthesis of aligned carbon nanotubes on double-sided metallic substrate by chemical vapor deposition. https://pubs.acs.org/doi/abs/10.1021/jp0730848, 2007.

[35] B.A. Cola, X. Xu, T.S. Fisher, Increased real contact in thermal interfaces: a carbon nanotube/foil material, Appl. Phys. Lett. 90 (2007), 093513, https://doi.org/10.1063/1.2644018. http://aip.scitation.org/doi/10.1063/1.2644018.

[36] J.R. Wasniewski, D.H. Altman, S.L. Hodson, T.S. Fisher, A. Bulusu, S. Graham, B. A. Cola, Characterization of metallically bonded carbon nanotube-based thermal interface materials using a high accuracy 1D steady-state technique, J. Electron. Packag. 134 (2012), 020901, https://doi.org/10.1115/1.4005909. http://electronicpackaging.asmedigitalcollection.asme.org/article.aspx?doi=10.1115/1.4005909.

[37] J. Hansson, M.K. Samani, A. Nylander, L. Ye, N. Wang, T. Nilsson, J. Liu, Synthesis of a graphene carbon nanotube hybrid film by joule self-heating CVD for thermal applications, in: IEEE 68th Electronic Components and Technology Conference (ECTC), IEEE, 2018, pp. 2450–2456, https://doi.org/10.1109/ECTC.2018.00369, 2018, https://ieeexplore.ieee.org/document/8429882/.

[38] M. Kumar, Y. Ando, Chemical vapor deposition of carbon nanotubes: a review on growth mechanism and mass production, J. Nanosci. Nanotechnol. 10 (2010) 3739–3758, https://doi.org/10.1166/jnn.2010.2939. http://openurl.ingenta.com/content/xref?genre=article&issn=1533-4880&volume=10&issue=6&spage=3739.

[39] S. Sun, M.K. Samani, Y. Fu, T. Xu, L. Ye, M. Satwara, K. Jeppson, T. Nilsson, L. Sun, J. Liu, Improving thermal transport at carbon hybrid interfaces by covalent bonds, Advanced Materials Interfaces 5 (2018) 1–9, https://doi.org/10.1002/admi.201800318.

[40] K.S. Novoselov, A.K. Geim, S.V. Morozov, D. Jiang, Y. Zhang, S.V. Dubonos, I. V. Grigorieva, A.A. Firsov, Electric field effect in atomically thin carbon films, science 306 (2004) 666–669, https://doi.org/10.1126/science.1102896.

[41] K.C. Ng, S. Zhang, C. Peng, G.Z. Chen, Individual and bipolarly stacked asymmetrical aqueous supercapacitors of cnts/sno2 and cnts/mno2 nanocomposites, J. Electrochem. Soc. 156 (2009) A846–A853, https://doi.org/10.1149/1.3205482.

[42] A. Lewandowski, M. Jakobczyk, M. Galinski, M. Biegun, Self-discharge of electrochemical double layer capacitors, Phys. Chem. Chem. Phys. 15 (2013) 8692–8699, https://doi.org/10.1039/C3CP44612C.

[43] M. Xia, J. Nie, Z. Zhang, X. Lu, Z.L. Wang, Suppressing self-discharge of supercapacitors via electrorheological effect of liquid crystals, Nanomater. Energy 47 (2018) 43–50, https://doi.org/10.1016/j.nanoen.2018.02.022.

[44] Z. Wang, X. Chu, Z. Xu, H. Su, C. Yan, F. Liu, B. Gu, H. Huang, D. Xiong, H. Zhang, et al., Extremely low self-discharge solid-state supercapacitors via the confinement effect of ion transfer, J. Mater. Chem. 7 (2019) 8633–8640, https://doi.org/10.1039/C9TA01028A.

[45] B.E. Conway, Electrochemical Supercapacitors: Scientific Fundamentals and Technological Applications, Springer Science & Business Media, 2013.

[46] K. Ge, G. Liu, Suppression of self-discharge in solid-state supercapacitors using a zwitterionic gel electrolyte, Chem. Commun. 55 (2019) 7167–7170, https://doi.org/10.1039/C9CC02424G.
[47] Y.J. Kang, H. Chung, C.-H. Han, W. Kim, All-solid-state flexible supercapacitors based on papers coated with carbon nanotubes and ionic-liquid-based gel electrolytes, Nanotechnology 23 (2012), 065401, https://doi.org/10.1088/0957-4484/23/28/289501.
[48] P. Chen, H. Chen, J. Qiu, C. Zhou, Inkjet printing of single-walled carbon nanotube/ruo 2 nanowire supercapacitors on cloth fabrics and flexible substrates, Nano Research 3 (2010) 594–603, https://doi.org/10.1007/s12274-010-0020-x.
[49] I.B. Dogru, M.B. Durukan, O. Turel, H.E. Unalan, Flexible supercapacitor electrodes with vertically aligned carbon nanotubes grown on aluminum foils, Prog. Nat. Sci.: Materials International 26 (2016) 232–236, https://doi.org/10.1016/j.pnsc.2016.05.011.
[50] Y.-S. Kim, K. Kumar, F.T. Fisher, E.-H. Yang, Out-of-plane growth of cnts on graphene for supercapacitor applications, Nanotechnology 23 (2011), 015301, https://doi.org/10.1088/0957-4484/23/1/015301.